HHS Public Access

Author manuscript

*J Control Release*. Author manuscript; available in PMC 2018 October 28.

Published in final edited form as:

*J Control Release*. 2017 October 28; 264: 160–168. doi:10.1016/j.jconrel.2017.08.029.

# ImmunoPET imaging of tissue factor expression in pancreatic cancer with $^{89}$Zr-Df-ALT-836

**Reinier Hernandez**[1], **Christopher G. England**[1], **Yunan Yang**[2], **Hector F. Valdovinos**[1], **Bai Liu**[3], **Hing C. Wong**[3], **Todd E. Barnhart**[1], and **Weibo Cai**[1,2,4,*]

[1]Department of Medical Physics, University of Wisconsin - Madison, WI 53705, USA

[2]Department of Radiology, University of Wisconsin - Madison, WI 53705, USA

[3]Altor Bioscience Corporation, Miramar, FL, 33025, USA

[4]University of Wisconsin Carbone Cancer Center, Madison, WI 53792, USA

## Abstract

Overexpression of tissue factor (TF) has been associated with increased tumor growth, tumor angiogenesis, and metastatic potential in many malignancies, including pancreatic cancer. Additionally, high TF expression was shown to strongly correlate with poor prognoses and decreased survival in pancreatic cancer patients. Herein, we exploited the potential targeting of TF for positron emission tomography (PET) imaging of pancreatic cancer. The TF-targeted tracer was developed through radiolabeling of the anti-human TF monoclonal antibody (ALT-836) with $^{89}$Zr. The tracer was characterized by fluorescence microscopy and flow cytometry assays in BXPC-3 and PANC-1 cells, two pancreatic cancer cell lines with high and low TF expression levels, respectively. Non-invasive PET scans were acquired in tumor-bearing mice injected with $^{89}$Zr-Df-ALT-836. Additionally, *ex vivo* biodistribution, blocking, and histological studies were performed to establish the affinity and specificity of $^{89}$Zr-Df-ALT-836 for TF *in vivo*. $^{89}$Zr-labeling of Df-ALT-836 was achieved in high yield and good specific activity. FACS and microscopy studies revealed no detectable difference in TF-binding affinity between ALT-836 and Df-ALT-836 *in vitro*. Longitudinal PET scans unveiled a lasting and prominent $^{89}$Zr-Df-ALT-836 uptake in BXPC-3 tumors (peak at 31.5 ± 6.0 %ID/g at 48 h post-injection; n=3), which was significantly abrogated (2.3 ± 0.5 %ID/g at 48 h post-injection; n=3) when mice were pre-injected with a blocking dose (50 mg/kg) of unlabeled ALT-836. *Ex vivo* biodistribution data confirmed the accuracy of the PET results, and histological analysis correlated high tumor uptake with *in situ* TF expression. Taken together, these results attest to the excellent affinity and TF-specificity of $^{89}$Zr-Df-ALT-836 *in vivo*. With elevated, persistent, and specific accumulation in TF-positive BXPC-3 tumors, PET imaging using $^{89}$Zr-Df-ALT-836 promises to open new avenues for improving future diagnosis, stratification, and treatment response assessment in pancreatic cancer patients.

*Corresponding Author: Weibo Cai, Ph.D., Address: Departments of Radiology and Medical Physics, University of Wisconsin – Madison, Room 7137, 1111 Highland Ave., Madison, WI 53705-2275, USA. wcai@uwhealth.org; Phone: 608-262-1749; Fax: 608-265-0614.

**Disclosure of Potential Conflicts of Interest**

B.L. and H.C.W. are employed by Altor Bioscience Corporation. No potential conflicts of interest were disclosed by the other authors.

**Keywords**

Tissue factor (TF); ALT-836; pancreatic cancer; $^{89}$Zr; positron emission tomography (PET); immunoPET; molecular imaging

## Introduction

Pancreatic cancer (PCa) is a devastating disease that, despite considerable research efforts, remains mostly incurable [1, 2]. Pancreatic carcinoma is a relatively uncommon condition with an incidence of approximately 50,000 new cases reported annually in the United States. In terms of mortality, it is the fourth leading cause of cancer-related deaths in both sexes, with the lowest 5-year survival rate (8%) among all major cancers. In this disease, patient survival greatly depends on the stage at diagnosis, with a 5-year survival that drops from 27% in localized malignancies to 2% when tumor dissemination is present. More importantly, the late onset of clinical symptoms results in more than 50% of patients being diagnosed with advanced stage PCa. This suggests that improvements in early detection of PCa could significantly improve overall patient survival. In consequence, finding effective methods for the noninvasive detection and accurate staging of PCa is of dire clinical importance. Detecting PCa with high sensitivity and specificity requires the identification of genotypic and phenotypic features present in tumors, yet absent in healthy tissues. In particular, the scrutiny of cell surface receptors expression, which may be accomplished noninvasively, has been proven highly valuable in the identification and classification of several malignancies [3–5].

Tissue factor (TF) is a transmembrane protein whose primary role is the initiation of the extrinsic blood coagulation cascade through binding and activation of coagulation serine protease factor VII/VIIa [6]. TF plays an essential role in homeostasis and its expression is largely confined to the vascular adventitia, organs capsules, and to a lesser extent in the cerebral cortex, renal glomeruli, and cardiac myocytes [7]. In cancer, TF overexpression has been linked to thrombosis, tumor angiogenesis, enhanced tumor growth, and metastasis [8, 9]. More specifically, the overexpression of TF in pancreatic cancer has been correlated with high tumor grade, extent of the primary disease, and local and distant metastatic invasion. Moreover, TF was proposed as an independent negative prognostic marker since low TF expression correlates with significantly improved patient survival. Lastly, TF is expressed at low levels in the normal pancreas, making it an optimal target for diagnosis and molecularly-targeted therapeutic intervention [10].

ALT-836, previously known as Sunol-cH36, is a chimeric monoclonal antibody (mAb) targeting human TF that is undergoing active investigation in clinical trials for the treatment of acute lung injury or respiratory distress syndrome. ALT-836 has been shown to interact with factor X/factor IX binding sites in human TF with nanomolar affinity, blocking activation of the coagulation cascade [11]. In this study, we exploit the excellent TF-targeting properties of ALT-836 and the ability of positron emission tomography (PET) to scrutinize the expression of biomarkers noninvasively *in vivo*, to generate a radiotracer that examines TF expression in PCa using immunoPET imaging. The positron-emitting

radiometal $^{89}$Zr was selected to radiolabel ALT-836 due to its amenable radiochemical properties and proven clinical relevance in the preparation of immunoconjugates for PET imaging [12]. The properties of $^{89}$Zr-Df-ALT-836 as a molecular imaging agent were evaluated via a series of *in vitro, ex vivo,* and *in vivo* imaging studies in mouse models of PCa, where we aimed to establish the potential of $^{89}$Zr-Df-ALT-836 for early detection, tumor staging, and evaluation of TF-targeted therapies in a future clinical setting.

## Materials and Methods

### Reagents

ALT-836 was kindly supplied by Altor Bioscience Corp. 1-(4-isothiocyanatophenyl)-3-[6,17-dihydroxy-7,10,18,21-tetraoxo-27-(N-acetylhydroxylamino)- 6,11,17, 22-tetraazaheptaeicosine] thiourea (p-SCN -Bn-Deferoxamine or Df) was purchased form Macrocyclics, Incorporation (Plano, TX) and Chelex 100 resin (50–100 mesh) was acquired from Sigma Aldrich (St. Louis, MO). Primary rat anti-mouse CD31 mAb was purchased for Novus Biologicals (Littleton, CO) and Alexafluor488 and Cy3-labeled secondary antibodies were procured by Jackson ImmunoResearch Laboratories (West Grove, PA). Milli-Q water (resistivity > 18.2 MΩ•cm) was employed in the preparation of all buffers and solutions. Buffers used for radiochemistry were treated with Chelex 100. The rest of the materials and reagents were purchase from Thermo Fisher Scientific Incorporation (Waltham, MA).

### Isotope production and radiochemistry

$^{89}$Zr was produced in a GE PETtrace biomedical cyclotron by irradiation of natural yttrium targets with 16.2 MeV protons. $^{89}$Zr was trapped in a hydroxamate-functionalized solid phase extraction column and eluted in 0.1 M oxalic acid. High $^{89}$Zr specific activities (SA) of ~110 GBq/μmol were attained. Deferoxamine (Df) was conjugated to free primary amine groups in ALT-836 of the lysine residues via formation of thiourea linkage. Briefly, ~5 mg (33 nmol) of ALT-836 in phosphate buffer saline (PBS; pH 7.4) was adjusted to pH 8.0–8.5 with $Na_2CO_3$ (0.1 M). Freshly dissolved p-SCN-Bz-Df in DMSO was added to the mixture in a 1:3 mAb:chelator molar ratio, and the pH was readjusted with $Na_2CO_3$ (0.1 M). The conjugation proceeded for 2 h at room temperature, after which the conjugated mAb (Df-ALT-836) was purified by size exclusion chromatography using PD-10 (GE Healthcare, Little Chalfont, United Kingdom) columns with PBS as the mobile phase. The number of Df chelators conjugated per antibody was determined through an isotopic dilution experiment following our previously reported methodology [13].

Radiolabeling of Df-ALT-836 with $^{89}$Zr was carried out following our standard procedure[14]. Approximately 121 MBq (3 mCi) of $^{89}$Zr-oxalate was adjusted to pH 7.0–7.5 in HEPES buffer (0.5 M) and 300 μg (100 μg/mCi) of Df-ALT-836 added to the reaction. After a 1 h incubation under constant shaking (500 rpm) at 37°C, $^{89}$Zr-Df-ALT-836 was purified via PD-10 columns. The radiochemical yield and purity was assessed by instant thin-layer chromatography (iTLC) using silica paper as stationary phase and 50 mM EDTA (pH 4.5) as the mobile phase. iTLC plates were developed in a cyclone phosphor-plate imager (Perkin Elmer, Waltham, MA) and the chromatograms were analyzed with the

OptiQuant software (Perkin Elmer). Free $^{89}$Zr moved with the solvent from ($R_f \approx 1.0$), whereas $^{89}$Zr-Df-ALT-836 remained at the point of spotting ($R_f \approx 0$).

## Cell culture

Two human pancreatic cancer cell lines, BXPC-3 and PANC-1, were obtained from the American Type Culture Collection (ATCC) and cultured according to the manufacturer's guidelines in a humidified incubator at 37 °C with 5% $CO_2$. Briefly, BXPC-3 and PANC-1 cells were cultured in Roswell Park Memorial Institute 1640 (RPMI-1640) medium and Dulbecco's Modified Eagle's medium (DMEM), respectively. Medium was supplemented with 10% fetal bovine serum (Thermo Fisher Scientific) and 1% penicillin-streptomycin solution (Gibco, Thermo Fisher Scientific).

## Animal Models

All animal studies were conducted under a protocol approved by the University of Wisconsin Institutional Animal Care and Use Committee. Cells were grown to 70% confluency before animal implantation. Five-week-old female athymic nude mice (Crl: NU(NCr)-Foxn1$^{nu}$; Envigo) were implanted subcutaneously with BXPC-3 or PANC-1 cells (1.5–2 × $10^6$ in 50% Matrigel; Corning). Tumors were monitored weekly and mice were utilized for imaging studies once tumors reached 100 – 150 $mm^3$ in volume.

## Flow cytometry

The binding of ALT-836 and DF-ALT-836 toward TF expressed in BXPC-3 and PANC-1 cell lines were determined by flow cytometry. BXPC-3 and PANC-1 cells were harvested and re-suspended in PBS with 1% bovine serum albumin (BSA) at 1 × $10^7$ cells/mL. The cells (100 μL/test) were incubated for 30 min at room temperature with PBS (control), 2$^{nd}$ antibody alone, ALT-836 (5 or 10 μg/mL), or Df-ALT-836 (5 or 10 μg/mL). Next, cells were washed with ice-cold PBS three times and followed by incubation with AlexaFluor488-labeled secondary antibody (5 μg/mL) for 30 min at room temperature. The MACSQuant cytometer (Miltenyi Biotech, Bergisch Gladbach, Germany) was used to run the samples and FlowJo analysis software (Tree Star, Inc) was used to process the data.

## Receptor density and competitive binding assay

Competitive binding and saturation binding assays were performed to determine the affinity of ALT-836 toward TF and to estimate the number of TF expressed on BXPC-3 cancer cells. For the competitive binding assay, 1×$10^5$ BXPC-3 cells were seeded into the wells of a filtered-bottom 96-well plate, and ~10,000 CPMs of $^{89}$Zr-Df-ALT-836 was added along with increasing concentrations of ALT-836 (range 0.1 nM – 333 nM). The plate was incubated for 2 h at room temperature under constant shaking, rinsed with cold PBS containing 0.1 % BSA, air-dried, and PVDF filters were collected and counted in an automatic gamma counter. ALT-836 competitive binding curves were plotted and analyzed using Prism (GraphPad Software, La Jolla, CA) software. In the saturation binding studies, increasing concentrations of $^{89}$Zr-Df-ALT-836 (range 0.01 nM – 100 nM; SA: 365 kBq/μmol) were added to the wells of a 96-well plate containing 1×$10^5$ BXPC-3 cells per well, and the plate was incubated for 2 h at room temperature. Next, the wells were rinsed with cold PBS/0.1 %

BSA and air-dried before the bottom filters were collected and counted. The saturation binding isotherms were plotted, and the TF-affinity constant ($K_d$) and receptor density were determined using Prism (GraphPad).

### Cell internalization assay

A cell internalization assay was performed to determine whether $^{89}$Zr-Df-ALT-836 was internalized or remained membrane-bound in BXPC-3 cells. To 24-well culture plates, $5\times10^5$ BXPC-3 cells were seeded and incubated in RPMI-1640 media overnight. After 12 h, the old media was replaced with 500 μL of fresh RPMI media containing 18.5 kBq (0.5 μCi) of $^{89}$Zr-Df-ALT-836 and 0.1% BSA, and the plates were incubated for 0.25, 0.5, 0.75, 1, 2, and 3 h at room temperature. At each timepoint, the supernatant was removed from the wells and an acid wash (0.1 M acetic acid, pH 2.5) was performed to remove membrane bound $^{89}$Zr-Df-ALT-836. Next, BXPC-3 cells were trypsinized and collected. Cell suspensions and acid wash fractions were counted in a gamma counter and the percentage of membrane bound versus internalized $^{89}$Zr-Df-ALT-836 was determined. We also determined the efflux of internalized $^{89}$Zr-Df-ALT-836. After a 2 h incubation, wells were rinsed with PBS containing 0.1% BSA, fresh RPMI media was added and then collected after a 0.25, 0.5, 0.75, 1, or 2 h incubation. Both BXPC-3 cells and supernatant radioactivity were measured and the percentage of efflux were calculated.

### PET imaging and ex vivo biodistribution

PET images were acquired using an Inveon micro-PET/CT scanner (Siemens Medical Solutions, Knoxville, TN). Mice bearing BXPC-3 (TF-positive) or PANC-1 (TF-negative) tumor xenografts (n = 3–4) were intravenously injected 7.4–11.1 MBq of $^{89}$Zr-Df-ALT-836. Before each PET scan, mice were anesthetized with isoflurane (2%) and place in prone position within the scanner. Sequential list mode PET scans of 40 million coincidence events each (time window: 3.432 ns; energy window: 350–650 keV) were acquired at 4, 24, 48, 72, and 120 h after the administration of the radiotracer. The PET images were reconstructed using a three-dimensional ordered subset expectation maximization (OSEM3D) algorithm. Quantitative region-of-interest analysis (ROI) of the images was performed in an Inveon Research Workplace workstation (Siemens Medical Solutions, Knoxville, TN) and $^{89}$Zr-Df-ALT-836 uptake in the different tissues was presented as percentage of injected dose per gram (%ID/g; mean ± SD). In a TF-blocking experiment, BXPC-3 mice (n = 4) were administered a large dose of unlabeled ALT-836 (50 mg/kg) 24 h prior to the injection of $^{89}$Zr-Df-ALT-836. PET scanning and image analysis were performed as described above. *Ex vivo* biodistribution was performed in all groups after the terminal imaging timepoint at 120 h post-injection of the tracer. Mice were euthanized and tissues of interest were harvested, wet-weighed, and counted in an automatic gamma counter (Wizard 2, Perking Elmer, MA). The results of the biodistribution were recorded as %ID/g (mean ± SD).

### Immunofluorescent staining

The expression of TF was evaluated by immunofluorescence staining following a previously described methodology [15]. After the terminal imaging timepoint, tissue samples form BXPC-3, PANC-1 tumors, and normal tissues including the liver, kidneys, and spleen were harvested, embedded in optimal cutting temperature (OCT) compound, frozen, and stored

for approximately 30 days (10 times $^{89}$Zr decay half-life) at −80 °C. Subsequently, 5 μm slices were cut from the specimens, fixed with acetone for 10 min, rinsed with PBS, blocked with 10% donkey serum for 30 min, and then incubated with a mixture of ALT-836 (5 μg/mL) and rat anti-mouse CD31 (5 μg/mL) monoclonal antibody at 4°C. Next, slides were washed before a 2 h incubation with the secondary antibodies, Alexa Fluor488-labeled goat antihuman IgG and Cy3-labeled donkey anti-rat IgG secondary antibodies (5 μg/mL). VectaShield Antifade Mounting Medium with DAPI for Fluorescence (Vector Laboratories, Burlingame, CA) was added to the slides before they were coverslipped and imaged using a Nikon Digital Eclipse C1 plus confocal fluorescence microscope.

### Tissue microarray staining and analysis

Human pancreatic cancer tissue microarrays containing samples from 91 patients were obtained from Biomax (Cat # PA961b; US Biomax, Inc., Rockville, MD, USA) and stained for TF expression using a protocol previously described [16]. Briefly, tissues were deparaffinized and hydrated through xylene and and a series of ethanol washes. Next, antigen retrieval was performed using the Vector Antigen Unmasking solution (Vector Laboratories, Burlingame, CA, USA). Slides were incubated in 2.5% normal horse serum for blocking using the Impress Reagent Kit Anti-Human IgG kit (Vector Laboratories, Burlingame, CA, USA) for 30 min at room temperature. After washing, slides were incubated with the primary antibody, ALT-836 for 12 h at 4 °C. Slides were washed in PBS and then incubated in 3% $H_2O_2$ for 5 min to block endogenous peroxidase. Next, the sections were incubated in diluted biotinylated secondary antibody (donkey anti-human) for 30 min at room temperature. Color formation occurred after incubation with the peroxidase substrate (ImmPACT VIP; Vector Laboratories, Burlingame, CA, USA) for 45 s. Slides were rinsed in tap water before counterstaining with Hematoxylin QS (Vector Laboratories, Burlingame, CA, USA) for 20 s. Lastly, slides were washed 5-times in tap water before applying the mounting medium and the coverslip. ImageJ was used to determine the relative staining intensity in comparison to control (healthy) tissues. Staining intensity values were assigned in 0.5 increments with 0 corresponding to the lowest degree of positive staining and 3.0 for the highest staining intensity. For each sample, four different stained location were analyzed and the average staining intensity was reported.

### Statistical Analysis

Quantitative data were expressed as mean ± standard deviation (SD). A student t-test was employed for significance using a confidence interval of 95%; a $p$-value of $<0.05$ was considered as statistically significant.

## RESULTS

### Radiotracer development

To enable the radiolabeling of $^{89}$Zr, the desferoxamine chelator was conjugated to the exposed lysine residues of ALT-836. Owing to our previous experience and the elevated specific activity (~121 GBq/μmol) of $^{89}$Zr-oxalate, approximately two Df were conjugated to each ALT-836. Radiolabeling with $^{89}$Zr was accomplished with excellent yields of ≥ 85%

and $^{89}$Zr-Df-ALT-836 radiochemical purity surpassed 95%. The averaged specific activity attained for the tracer was ~31 GBq/μmol.

## In vitro assays

Several *in vitro* assays were performed in BXPC-3 and PANC-1 to verify TF expression and to characterize the tracer's binding affinity, TF specificity, and cell internalization. The immunoreactivity of Df-ALT-836 was compared to that of native ALT-836 using flow cytometry (Figure 1A). As noted in the fluorescent histograms, both ALT-836 and Df-ALT-836 displayed similarly high binding to TF-positive BXPC-3 cells, whereas only background signal was detected in TF-negative PANC-1 cells. These results showed that conjugation of Df elicited no adverse effects on the binding properties of the tracer.

Quantitative measurements of Df-ALT-836 binding affinity were obtained in competitive and saturation binding assays using TF-expressing BXPC-3 cells. A competitive binding assay using $^{89}$Zr-Df-ALT-836 as the radioligand showed a 50% inhibition concentration ($IC_{50}$) of 1.38 ± 0.34 nM (Figure 1B). Similarly, the saturation binding isotherm revealed a TF binding affinity constant ($K_d$) of 1.49 ± 0.66 nM, which perfectly aligned with the competitive binding assays results (Figure 1C). Additionally, the maximum ligand binding ($B_{max}$) of BXPC-3 was determined to be 101.80 ± 9.87 fmol, which corresponded to a receptor density of 6.36 ± 0.59 × $10^5$ TF per cell. $^{89}$Zr-Df-ALT-836 displayed rapid internalization kinetics in BXPC-3 cells, with 33% of the total added activity being internalized within the first 3 h of incubation (Figure 1D). Membrane-bound $^{89}$Zr-Df-ALT-836 was low (~10%), as well as the efflux of internalized ligand (Figure 1D and E). Altogether, these studies revealed the excellent *in vitro* binding affinity and TF-specificity of Df-ALT-836 towards TF-expressing BXPC-3 cells.

## PET imaging

Noninvasive PET imaging was performed to corroborate the TF-targeting properties of $^{89}$Zr-Df-ALT-836 *in vivo*, and to determine the pharmacokinetic profile of the tracer in mice. The extended physical decay half-life of $^{89}$Zr ($t_{1/2}$: 78.4 h) allowed for the successful tracking of $^{89}$Zr-Df-ALT-836 biodistribution in tumor-bearing mice up to 5 days (120 h) after administration. Representative maximum intensity projection (MIP) PET images of mice bearing pancreatic cancer xenografts showed a clear delineation of TF-positive BXPC-3 tumors (Figure 2) as early as 3 h post-injection of the tracer. Conversely, tumor signal was markedly lower in mice bearing PANC-1 xenografts throughout the whole study.

These results were confirmed quantitatively via a region-of-interest (ROI) analysis of the PET images (Figure 3B and C). Consistent with the pharmacokinetic profile of radiolabeled mAbs [14, 17], $^{89}$Zr-Df-ALT-836 revealed high blood pool activities of 13.75 ± 1.60 %ID/g and 16.28 ± 0.85 %ID/g at the initial 4 h post administration timepoint in BXPC-3 and PANC-1 tumor bearing mice, respectively (n = 3–4). Further analysis of the image-derived time activity curves of the heart indicated a slow $^{89}$Zr-Df-ALT-836 clearance from circulation with similar half-lives of 11.23 ± 2.12 h and 14.81 ± 3.45 h in the BXPC-3 and PANC-1 groups, respectively. Prominent liver uptake of $^{89}$Zr-Df-ALT-836 was observed 4 h after injection in the BXPC-3 and PANC-1 groups (12.72 ± 1.34 %ID/g vs 18.97

± 0.93 %ID/g), which experienced a limited decline in magnitude (9.13 ± 1.44 %ID/g vs 16.50 ± 2.90 %ID/g), 120 h after tracer administration (n = 3–4). $^{89}$Zr-Df-ALT-836 uptake in non-target tissues, such as muscle, remained at low levels (< 1 %ID/g). In accordance with the *in vitro* results, $^{89}$Zr-Df-ALT-836 tumor uptake was significantly greater in BXPC-3 xenografts compared to PANC-1. Prominent tracer uptake in BXPC-3 tumors was observed from the initial timepoint (14.65 ± 2.81 %ID/g, at 4 h post-injection) and steadily increased to a peak value of 31.50 ± 6.00 %ID/g by 48 h post-injection of $^{89}$Zr-Df-ALT-836 (n = 4). Minimal radiotracer wash-out from BXPC-3 tumors was observed for 120 h following administration, as tumors remained the tissue with the highest activity accumulation (26.55 ± 3.60 %ID/g). On other hand, TF-negative PANC-1 tumors presented significantly lower $^{89}$Zr-Df-ALT-836 uptake ($p < 0.001$), with a maximum of 5.77 ± 0.76 %ID/g at 48 h post-injection. Of note was the marginal PET signal detected in bone, even at delayed imaging timepoints, which pointed to the superior *in vivo* stability of the radiotracer.

A significant reduction in tumor radioactivity was observed when mice bearing BXPC-3 xenografts were intravenously administered a large dose of unlabeled ALT-836 (50 mg/kg), 24 h prior to the injection of $^{89}$Zr-Df-ALT-836. Blocking of TF resulted in the abrogation of more than 90% in peak BXPC-3 tumor uptake (31.50 ± 6.00 vs. 2.68 ± 0.77 %ID/g; n = 4) and an overall statistically significant reduction across all timepoints ($p < 0.001$). $^{89}$Zr-Df-ALT-836 uptake in blocked non-target tissues and clearance organs was slightly different compared to the non-blocked BXPC-3 and PANC-1 groups (Table S1). Overall, results of the *in vivo* PET imaging studies demonstrated that $^{89}$Zr-Df-ALT-836 could detect the differential expression of TF noninvasively with excellent specificity in pancreatic cancer.

## Ex vivo biodistribution

Following the final imaging timepoint at 120 h post-injection, a whole-body biodistribution study was performed, in which mice were euthanized and all major organs harvested for *ex vivo* gamma counting. The goal of this study was to corroborate the accuracy of the image-derived quantitative PET data and to describe the biodistribution of $^{89}$Zr-Df-ALT-836 in a more detailed manner (Figure 4, Table S2). Excellent congruence was found between the 120 h post-injection quantitative PET and *ex vivo* data, in both magnitude and trend. Radiotracer uptake was significantly higher in TF-positive BXPC-3 tumors compared to TF-negative PANC-1 (19.16 ± 5.37 vs. 5.20 ± 0.65 %ID/g; $P < 0.001$; n = 3–4). TF blocking resulted in an expected drastic reduction in $^{89}$Zr-Df-ALT-836 tumor uptake compared to the unblocked BXPC-3 group (19.16 ± 5.37 vs. 0.97 ± 0.50 %ID/g; $P < 0.001$; n = 4). Besides the moderate uptake in the liver, spleen, and kidneys, the remaining non-target normal tissues all showed low tracer accretion (< 5%ID/g). Given the bone-seeking nature of transchelated $^{89}$Zr *in vivo*, uptake in the bones was quantified. Bone radioactivity was 5.94 ± 1.88, 6.04 ± 2.42, and 2.24 ± 2.12 %ID/g in the BXPC-3, PANC-1, and TF blocking groups, respectively, values that are comparable to those reported using other $^{89}$Zr-labeled antibodies [13, 18]. In general, the analysis of the *ex vivo* tissue distribution confirmed the accuracy of the image-derived data, suggesting the value of $^{89}$Zr-Df-ALT-836 for noninvasive PET imaging of TF expression.

### Histology

TF (green channel) and CD31 (red channel) immunofluorescence co-staining was performed in BXPC-3 and PANC-1 tumors, liver, spleen, and kidney tissue sections (Figure 5). An intense green fluorescence signal was observed in BXPC-3 tumor slices consistent with an elevated *in situ* expression of TF. On the other hand, PANC-1 tumor sections showed minimal fluorescent staining that is indicative of lower TF expression. Despite displaying noticeable levels of $^{89}$Zr-Df-ALT-836 uptake as seen by PET, the liver, spleen, and kidney tissue sections presented background levels of TF expression, which demonstrated the largely non-specific character of the tracer accumulation in these organs (i.e. mostly due to tracer clearance). The results of immunofluorescence studies successfully linked tumor $^{89}$Zr-Df-ALT-836 uptake with the levels of *in situ* TF expression and verified the TF-specificity of the radiotracer.

### Staining of TF in human pancreatic cancer tissue microarray

Expression of TF was examined in different types of pancreatic cancer using human tissue microarrays (Figure 6). After the tissue microarrays had been stained for TF expression, staining intensity was analyzed and quantified from 0 to 3.0 as described in the methods section. While expression varied between each cancer subtype, the values were significantly higher that of normal pancreatic tissues (Figure 6A). Adenocarcinomas, squamous cell carcinomas, solid pseudopapillary carcinomas, and neuroendocrine carcinomas displayed TF staining intensity values of $1.34 \pm 0.30$, $1.81 \pm 0.23$, $2.25 \pm 0.12$, and $2.13 \pm 0.31$, respectively. As the control, healthy pancreatic tissue showed minimal TF expression that was scored as $0.20 \pm 0.06$. Representative images depicting each pancreatic tumor subtype are provided in Figure 6B.

## Discussion

Despite decades of intense preclinical and clinical research, pancreatic cancer remains a highly lethal disease. Innumerable difficulties are associated with the diagnosis and treatment of PCa, making it one of the hardest cancers to detect and manage [19]. During early stage, PCa is a silent disease with only few specific symptoms, which results in most patients (80 – 85%) being diagnosed with advanced stage disease [20, 21]. Even the small percentage (10–20%) of patients diagnosed with early stage disease that undergo surgical resection still show dismal survival rates with most patients progressing with a median survival of less than two years. The fact of the matter is that PCa is a highly heterogeneous disease comprising of a myriad of genetic alteration, typically occurring at a low frequency, which makes the implementation of biomarker-based diagnostics and targeted therapies very challenging. To date, the lack of reliable serum biomarkers in combination with the low incidence of PCa renders population-wide screenings impractical [22–24]. The discovery of new biomarkers and targets for therapy are necessary to exert opportune interventions in patients with PCa. Parallel to the discovery of molecular targets, there is a pressing need for alternative noninvasive strategies for improved detection of pancreatic malignancies. In that regard, imaging technologies such as contrast-enhanced computed tomography (CE-CT) and magnetic resonance imaging (MRI) are becoming indispensable for early detection of PCa. From those, combined PET/CT offers improved sensitivity compared to other imaging

modalities [25]. In this study, we sought to couple the excellent binding affinity and TF-specificity of the mAb ALT-836 with the high sensitivity and quantitation capabilities of PET to scrutinize the *in vivo* expression of TF in murine models of pancreatic cancer, and achieved excellent results as detailed above.

New evidence of the vital role of TF in the aberrant homeostasis of cancer is constantly emerging. Overexpression of TF has been linked to thrombotic complications, known as Trousseau syndrome, which is ubiquitous to cancer patients [8]. Additionally, TF has been associated with tumor growth, tumor angiogenesis, and metastasis through several mechanisms including the activation of protease-activated receptor 2 (PAR2) and the TF-induced overexpression of vascular endothelial growth factor (VEGF) [8, 26]. These mechanisms are particularly exacerbated in pancreatic cancer where TF expression has been correlated with elevated VEGF expression, increased microvessel density, and venous thromboembolism [10]. The expression of TF has been detected in a large proportion of resected pancreatic cancer tissues, where high TF expression constitutes a negative predictor of survival. Additionally, TF-negative PCa patients are typically associated with a significantly better prognosis, even in those presenting with metastatic disease [6]. Moreover, the expression of TF in PCa occurs at the early stages of the neoplastic transformation, making it promising biomarker for early diagnosis and timely therapeutic intervention [10].

Despite the body of evidence correlating TF expression with tumor aggressiveness, metastasis, and an overall poor patient performance, the targeting of TF has been underexploited for targeted diagnosis and therapy of PCa. Particularly, since the limited examples of therapeutic studies inhibiting TF have shown promise in preclinical models of breast, prostate, and lung cancer [27–29]. The chimeric mAb, ALT-836, has been demonstrated to bind TF with excellent affinity and effectively inhibit the TF functional pathway by preventing the formation of the TF:FVIIa complex. Moreover, the safety profile of ALT-836 has been clinically demonstrated in patients with acute lung injury and acute respiratory distress syndrome (ALI/ARDS) [30], and it is currently being evaluated in phase 1 clinical trial (ClinicalTrials.gov; NCT01325558) for the treatment of solid tumors in combination with gemcitabine. Such mounting evidence on the potential clinical impact of ALT-836-based therapies in PCa highlights the potential relevance of an ALT-836-based molecular imaging agents. In a future clinical setting, such tracers may facilitate the screening of eligible TF-expressing patients to undergo more aggressive targeted therapeutic approaches, as well as to monitor the efficacy of such strategies.

$^{89}$Zr-Df-ALT-836 performed effectively *in vivo*, as tumors of mice bearing TF-positive BXPC-3 xenografts were readily delineated, owing to the high tumor-to-normal tissue contrasts attained. The ability of $^{89}$Zr-Df-ALT-836 to detect differences in TF expression *in vivo* was evidenced by the significantly higher tumor uptake values observed in BXPC-3 tumors compare to their TF-negative counterparts PANC-1. Additionally, the TF-specific character of the tumor accretion was confirmed in a receptor blocking study, where injection of a TF-saturating dose of unlabeled mAb greatly reduced the tumor uptake of $^{89}$Zr-Df-ALT-836. The different levels of tumor radioactivity correlated well with *in situ* TF expression determined by *ex vivo* immunofluorescent staining of resected tumor sections,

indicating the reliability of $^{89}$Zr-Df-ALT-836 immunoPET for assessing TF expression *in vivo*. Overall, $^{89}$Zr-Df-ALT-836 exhibited excellent properties as radiotracer for immunoPET imaging of TF in PCa.

Due to limitations on its decay properties - $^{64}$Cu has a decay half-life of 12.7 h - our previous TF-targeting tracer $^{64}$Cu-NOTA-ALT-836, could not track the fate of the tracer *in vivo* beyond 48 h after administration since [31]. In contrast, given the longer decay half-live of $^{89}$Zr, $^{89}$Zr-Df-ALT-836 allowed for the long-term tracking of tracer biodistribution, fully capturing the tumor time-activity curve and the hepatobiliary clearance of the antibody. This certainly facilitates the estimation of the radiotracer dosimetry, as well as the planning of potential targeted radiotherapy approaches. On another note, a common drawback of using of $^{89}$Zr as PET isotope, is the bone-seeking character of this metal in its weakly chelated form. Evidence of bone depositions was observed in the PET images starting at day 2 after tracer infusion, and it was later confirmed by *ex vivo* biodistribution studies at the 120 h post-injection timepoint. Nonetheless, bone uptake was around 6 %ID/g or lower in all groups, values that are modest compared to those of other registered $^{89}$Zr-labeled biomolecules [32], which further demonstrated the superior radiostability of the tracer *in vivo*.

A standing and incredibly crucial question to our studies is the extrapolation of our animal results to more realistic clinical scenario. The relevance of cancer cell lines and their derived tumor xenografts in biological studies has recently come into question, as cell lines may display different genotypic and phenotypic properties than what is found in human tumors. To determine the relevance of TF expression in real PCa patient populations, and the ability of ALT-836 to scrutinize it, we carried out a histological survey of TF expression in human PCa tissue microarrays, using ALT-836 as the primary antibody. We observed medium to elevated TF expression (score 1–3) in a significant fraction of the analyzed pancreatic cancer tissue samples, findings that were consistent with those described in the Human Protein Atlas database reporting medium or high TF expression in more than 80% of the stained samples [33]. The low staining intensity found in the healthy pancreatic sections in our tissue microarrays was consistent with a basal expression of TF observed in some exocrine glandular cells of the human pancreas (Figure 6B). Altogether, these data further validate our hypothesis that TF may serve as a valuable biomarker for non-invasive imaging in pancreatic cancer. As differences exist in terms of tumor burden, dosing, and pharmacokinetic and pharmacodynamic profiles of antibodies between rodents and man, further clinical investigation is warranted to validate our promising results in humans.

## Conclusions

In this study, we have successfully developed a radiotracer for noninvasive immunoPET imaging of *in vivo* TF expression in pancreatic cancer. Owing to a high binding affinity and TF-specificity, $^{89}$Zr-Df-ALT-836 displayed elevated and persistent accumulation in the tumors of mice bearing BXPC-3 xenografts. Additionally, we could correlate tracer uptake with the levels of TF expression through various *in vitro*, *in vivo*, and *ex vivo* studies. More importantly, the staining of human pancreatic cancer tissue microarrays unveiled the prevalence of TF expression in pancreatic cancer, highlighting the potential usefulness of

TF-targeting for imaging and therapy of this disease. These encouraging results warrant further exploration towards the clinical implementation of TF-targeting, not only in pancreatic cancer but to other ailments where TF overexpression plays a vital role in the disease.

## Supplementary Material

Refer to Web version on PubMed Central for supplementary material.

## Acknowledgments

This work was supported in part by the University of Wisconsin - Madison, the National Institutes of Health (NIBIB/NCI 1R01CA169365, P30CA014520, T32CA009206, and T32GM008349), the National Science Foundation (DGE-1256259), and the American Cancer Society (125246-RSG-13-099-01-CCE).

## References

1. Siegel RL, Miller KD, Jemal A. Cancer statistics, 2016. CA Cancer J Clin. 2016; 66:7–30. [PubMed: 26742998]
2. A.C. Society. Cancer Facts & Figures 2016. American Cancer Society; Atlanta: 2016.
3. van Dongen GA, Visser GW, Lub-de Hooge MN, de Vries EG, Perk LR. Immuno-PET: a navigator in monoclonal antibody development and applications. Oncologist. 2007; 12:1379–1389. [PubMed: 18165614]
4. O'Shannessy DJ, Yu G, Smale R, Fu YS, Singhal S, Thiel RP, Somers EB, Vachani A. Folate receptor alpha expression in lung cancer: diagnostic and prognostic significance. Oncotarget. 2012; 3:414–425. [PubMed: 22547449]
5. De Abreu FB, Wells WA, Tsongalis GJ. The emerging role of the molecular diagnostics laboratory in breast cancer personalized medicine. Am J Pathol. 2013; 183:1075–1083. [PubMed: 23920325]
6. Nitori N, Ino Y, Nakanishi Y, Yamada T, Honda K, Yanagihara K, Kosuge T, Kanai Y, Kitajima M, Hirohashi S. Prognostic significance of tissue factor in pancreatic ductal adenocarcinoma. Clin Cancer Res. 2005; 11:2531–2539. [PubMed: 15814630]
7. Drake TA, Morrissey JH, Edgington TS. Selective cellular expression of tissue factor in human tissues. Implications for disorders of hemostasis and thrombosis. Am J Pathol. 1989; 134:1087–1097. [PubMed: 2719077]
8. Kasthuri RS, Taubman MB, Mackman N. Role of tissue factor in cancer. J Clin Oncol. 2009; 27:4834–4838. [PubMed: 19738116]
9. van den Berg YW, Osanto S, Reitsma PH, Versteeg HH. The relationship between tissue factor and cancer progression: insights from bench and bedside. Blood. 2012; 119:924–932. [PubMed: 22065595]
10. Khorana AA, Ahrendt SA, Ryan CK, Francis CW, Hruban RH, Hu YC, Hostetter G, Harvey J, Taubman MB. Tissue factor expression, angiogenesis, and thrombosis in pancreatic cancer. Clin Cancer Res. 2007; 13:2870–2875. [PubMed: 17504985]
11. Jiao JA, Kelly AB, Marzec UM, Nieves E, Acevedo J, Burkhardt M, Edwards A, Zhu XY, Chavaillaz PA, Wong A, Wong JL, Egan JO, Taylor D, Rhode PR, Wong HC. Inhibition of acute vascular thrombosis in chimpanzees by an anti-human tissue factor antibody targeting the factor X binding site. Thromb Haemost. 2010; 103:224–233. [PubMed: 20062929]
12. Wright BD, Lapi SE. Designing the magic bullet? The advancement of immuno-PET into clinical use. J Nucl Med. 2013; 54:1171–1174. [PubMed: 23908265]
13. Hernandez R, Sun H, England CG, Valdovinos HF, Ehlerding EB, Barnhart TE, Yang Y, Cai W. CD146-targeted immunoPET and NIRF Imaging of Hepatocellular Carcinoma with a Dual-Labeled Monoclonal Antibody. Theranostics. 2016; 6:1918–1933. [PubMed: 27570560]

14. Hernandez R, Sun H, England CG, Valdovinos HF, Barnhart TE, Yang Y, Cai W. ImmunoPET Imaging of CD146 Expression in Malignant Brain Tumors. Mol Pharm. 2016; 13:2563–2570. [PubMed: 27280694]
15. Yang Y, Hernandez R, Rao J, Yin L, Qu Y, Wu J, England CG, Graves SA, Lewis CM, Wang P, Meyerand ME, Nickles RJ, Bian XW, Cai W. Targeting CD146 with a 64Cu-labeled antibody enables in vivo immunoPET imaging of high-grade gliomas. Proc Natl Acad Sci U S A. 2015; 112:E6525–6534. [PubMed: 26553993]
16. Sun H, England CG, Hernandez R, Graves SA, Majewski RL, Kamkaew A, Jiang D, Barnhart TE, Yang Y, Cai W. ImmunoPET for assessing the differential uptake of a CD146-specific monoclonal antibody in lung cancer. Eur J Nucl Med Mol Imaging. 2016; 43:2169–2179. [PubMed: 27342417]
17. Wang W, Wang EQ, Balthasar JP. Monoclonal antibody pharmacokinetics and pharmacodynamics. Clin Pharmacol Ther. 2008; 84:548–558. [PubMed: 18784655]
18. Abou DS, Ku T, Smith-Jones PM. In vivo biodistribution and accumulation of 89Zr in mice. Nucl Med Biol. 2011; 38:675–681. [PubMed: 21718943]
19. Kleeff J, Korc M, Apte M, La Vecchia C, Johnson CD, Biankin AV, Neale RE, Tempero M, Tuveson DA, Hruban RH, Neoptolemos JP. Pancreatic cancer. Nat Rev Dis Primers. 2016; 2:16022. [PubMed: 27158978]
20. Hidalgo M, Cascinu S, Kleeff J, Labianca R, Lohr JM, Neoptolemos J, Real FX, Van Laethem JL, Heinemann V. Addressing the challenges of pancreatic cancer: future directions for improving outcomes. Pancreatology. 2015; 15:8–18. [PubMed: 25547205]
21. Vincent A, Herman J, Schulick R, Hruban RH, Goggins M. Pancreatic cancer. Lancet. 2011; 378:607–620. [PubMed: 21620466]
22. Misek DE, Patwa TH, Lubman DM, Simeone DM. Early detection and biomarkers in pancreatic cancer. J Natl Compr Canc Netw. 2007; 5:1034–1041. [PubMed: 18053427]
23. Swords DS, Firpo MA, Scaife CL, Mulvihill SJ. Biomarkers in pancreatic adenocarcinoma: current perspectives. Onco Targets Ther. 2016; 9:7459–7467. [PubMed: 28003762]
24. Greer JB, Brand RE. Screening for pancreatic cancer: current evidence and future directions. Gastroenterol Hepatol (N Y). 2007; 3:929–938. [PubMed: 21960811]
25. Sahani DV, Bonaffini PA, Catalano OA, Guimaraes AR, Blake MA. State-of-the-art PET/CT of the pancreas: current role and emerging indications. Radiographics. 2012; 32:1133–1158. discussion 1158–1160. [PubMed: 22786999]
26. Schaffner F, Versteeg HH, Schillert A, Yokota N, Petersen LC, Mueller BM, Ruf W. Cooperation of tissue factor cytoplasmic domain and PAR2 signaling in breast cancer development. Blood. 2010; 116:6106–6113. [PubMed: 20861457]
27. Cole M, Bromberg M. Tissue factor as a novel target for treatment of breast cancer. Oncologist. 2013; 18:14–18. [PubMed: 23287882]
28. Cheng J, Xu J, Duanmu J, Zhou H, Booth CJ, Hu Z. Effective treatment of human lung cancer by targeting tissue factor with a factor VII-targeted photodynamic therapy. Curr Cancer Drug Targets. 2011; 11:1069–1081. [PubMed: 21933104]
29. Hu Z, Garen A. Targeting tissue factor on tumor vascular endothelial cells and tumor cells for immunotherapy in mouse models of prostatic cancer. Proc Natl Acad Sci U S A. 2001; 98:12180–12185. [PubMed: 11593034]
30. Morris PE, Steingrub JS, Huang BY, Tang S, Liu PM, Rhode PR, Wong HC. A phase I study evaluating the pharmacokinetics, safety and tolerability of an antibody-based tissue factor antagonist in subjects with acute lung injury or acute respiratory distress syndrome. BMC Pulm Med. 2012; 12:5. [PubMed: 22340260]
31. Hong H, Zhang Y, Nayak TR, Engle JW, Wong HC, Liu B, Barnhart TE, Cai W. Immuno-PET of tissue factor in pancreatic cancer. J Nucl Med. 2012; 53:1748–1754. [PubMed: 22988057]
32. England CG, Kamkaew A, Im HJ, Valdovinos HF, Sun H, Hernandez R, Cho SY, Dunphy EJ, Lee DS, Barnhart TE, Cai W. ImmunoPET Imaging of Insulin-Like Growth Factor 1 Receptor in a Subcutaneous Mouse Model of Pancreatic Cancer. Mol Pharm. 2016; 13:1958–1966. [PubMed: 27054683]
33. Uhlen M, Fagerberg L, Hallstrom BM, Lindskog C, Oksvold P, Mardinoglu A, Sivertsson A, Kampf C, Sjostedt E, Asplund A, Olsson I, Edlund K, Lundberg E, Navani S, Szigyarto CA,

Odeberg J, Djureinovic D, Takanen JO, Hober S, Alm T, Edqvist PH, Berling H, Tegel H, Mulder J, Rockberg J, Nilsson P, Schwenk JM, Hamsten M, von Feilitzen K, Forsberg M, Persson L, Johansson F, Zwahlen M, von Heijne G, Nielsen J, Ponten F. Proteomics. Tissue-based map of the human proteome. Science. 2015; 347:1260419. [PubMed: 25613900]

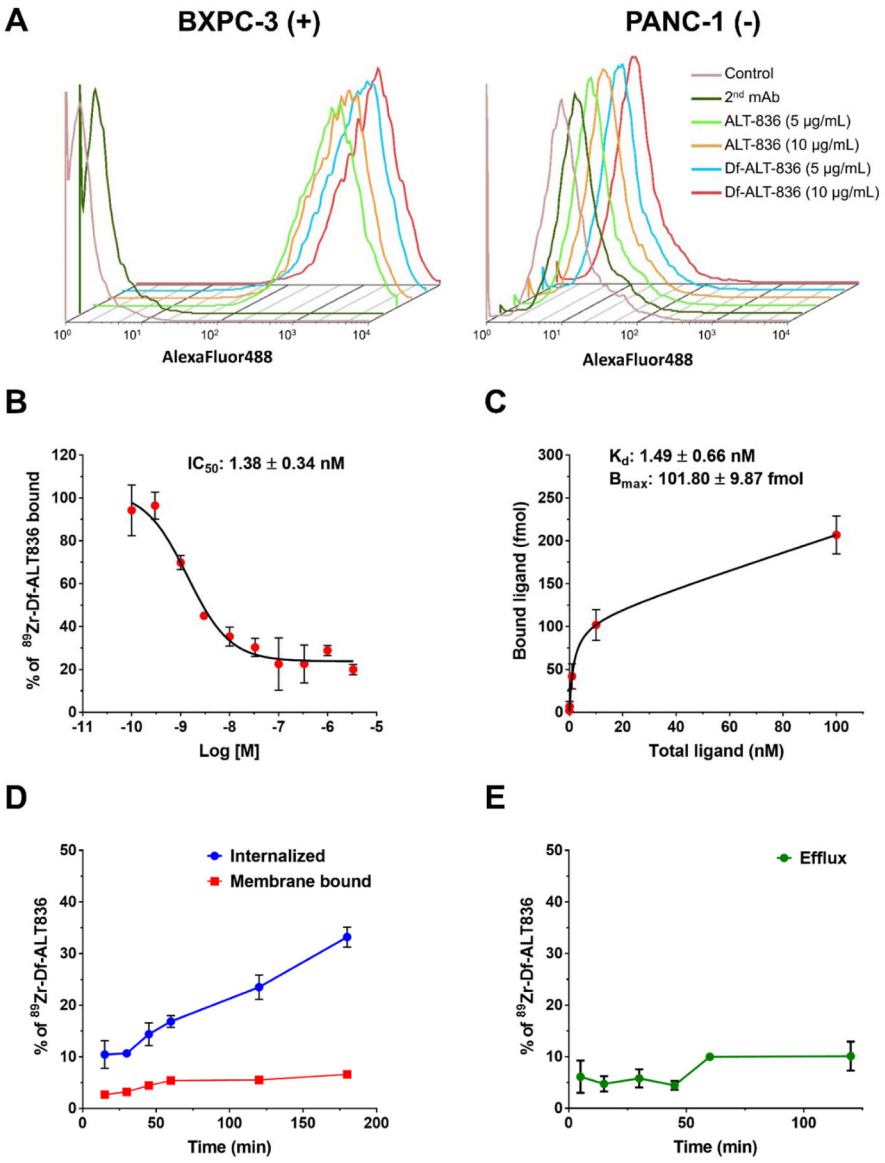


**Figure 1.**

*In vitro* characterization of $^{89}$Zr-Df-ALT-836. **(A)** Flow cytometry analysis of TF-binding of ALT-836 and Df-ALT-836 in BXPC-3 (TF-high) and PANC-1 (TF-low) human pancreatic cancer cells. **(B)** Concentration-depended displacement of bound $^{89}$Zr-Df-ALT-836 by Df-ALT-836 in BXPC-3 cells ($IC_{50}$: 1.38 ± 0.34 nM). **(C)** TF saturation binding assay curve in BXPC-3 cells. The TF-affinity constant of $^{89}$Zr-Df-ALT-836 ($K_d$: 1.49 ± 0.66 nM) and the number of TF per cell ($6.36\times10^5$) were determined. **(D)** Cell internalization assay displaying the kinetics of $^{89}$Zr-Df-ALT-836 **(E)** and efflux in BXPC-3 cancer cells.

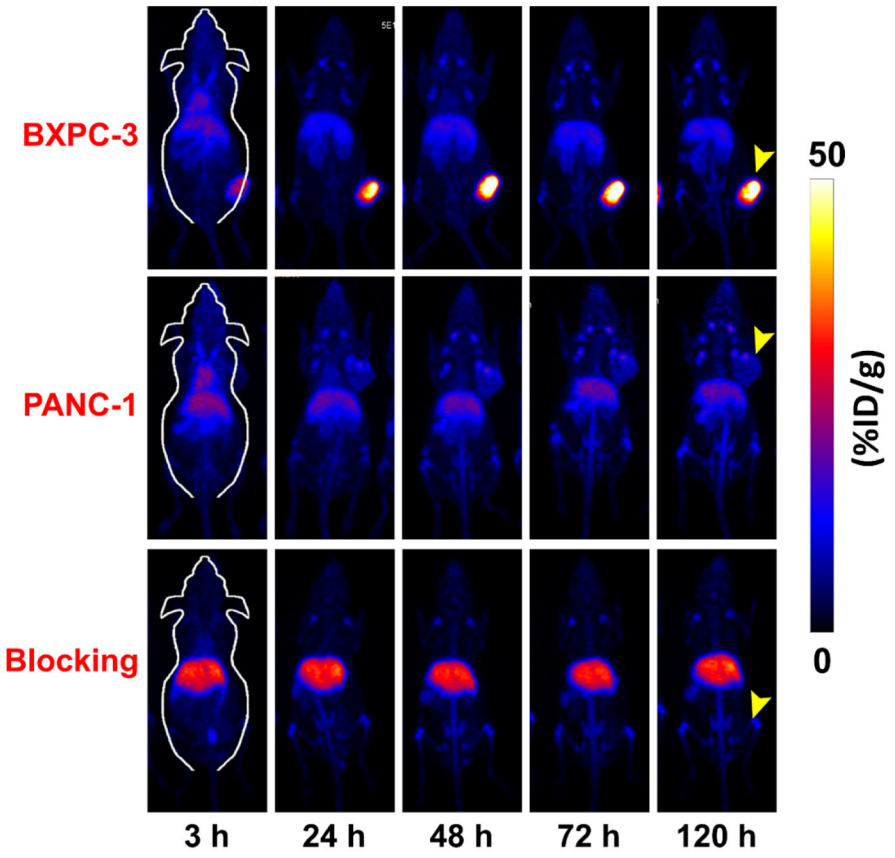


**Figure 2.**

Representative maximum-intensity projection (MIP) of longitudinal *in vivo* PET images of pancreatic cancer-bearing mice administered $^{89}$Zr-Df-ALT-836 (7.4–11.1 MBq). Prominent tumor uptake of $^{89}$Zr-Df-ALT-836 was observed in mice bearing BXPC-3 xenografts (top row), while PANC-1 tumors (middle row) exhibited negligible radioactivity accumulation. Mice pre-injected with a TF-blocking dose of ALT-836 (50 mg/kg) displayed significantly lower accrual of the tracer in BXPC-3 tumors (bottom row).

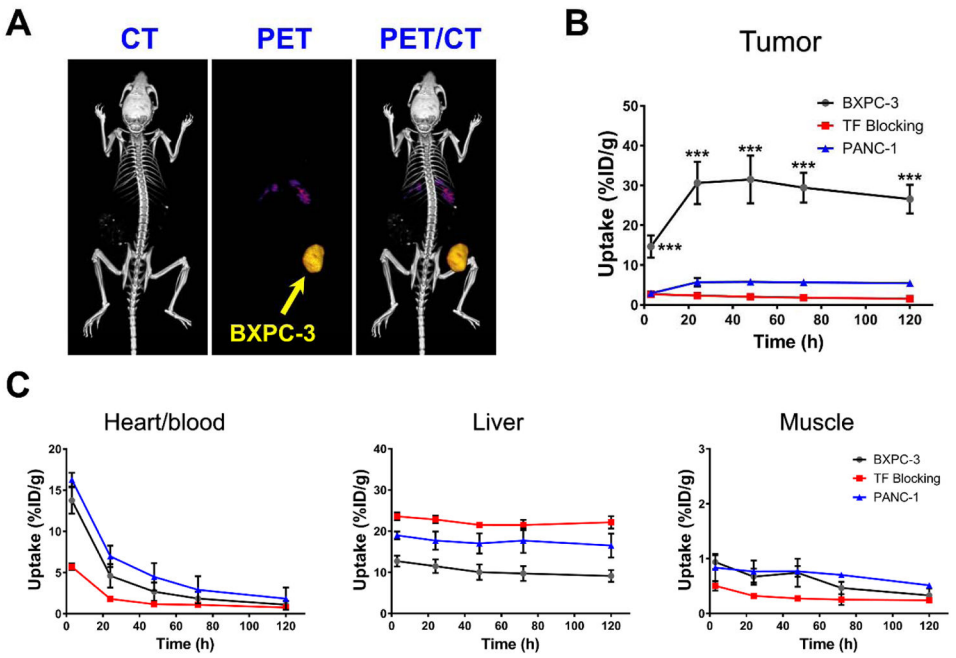


**Figure 3.**

Quantitative analysis of longitudinal PET images. **(A)** Representative 3D rendering of PET/CT images acquired in mice administered $^{89}$Zr-Df-ALT-836 at 48 h post-injection. **(B)** Time-activity curves (TACs) describing $^{89}$Zr-Df-ALT-836 uptake in mice bearing BXPC-3, PANC-1, and TF-blocked BXPC-3 xenografts. Uptake of the tracer was significantly higher in BXPC-3 tumors at all timepoints. **(C)** TACs describing the clearance of the tracer from heart/blood, liver, and muscle. Quantitative data was generated from a region-of-interest analysis of the PET images and reported as %ID/g (mean ± SD).

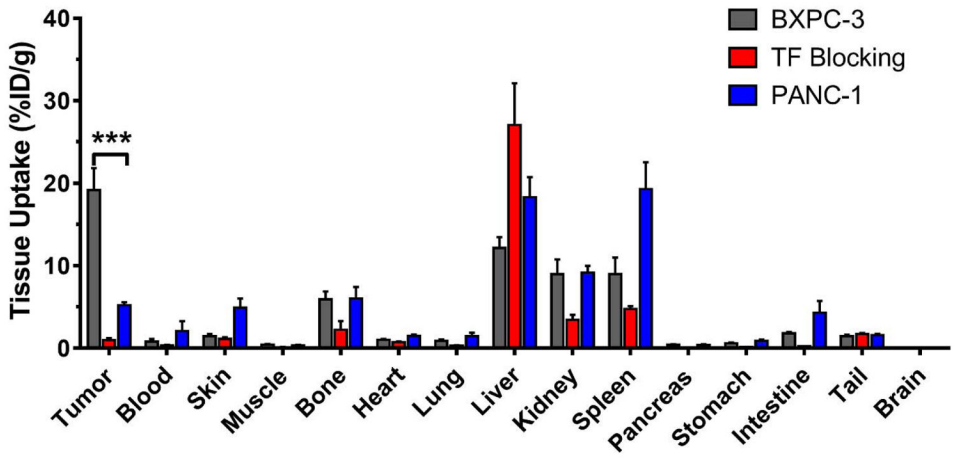


**Figure 4.**

*Ex vivo* biodistribution of $^{89}$Zr-Df-ALT-836 in mice bearing BXPC-3 or PANC-1 tumor xenografts. Mice were euthanized 120 h after injection of $^{89}$Zr-Df-ALT-836 and tracer biodistribution in the tumor and normal tissues was determined via gamma counting. Results were expressed as %ID/g (mean ± SD).

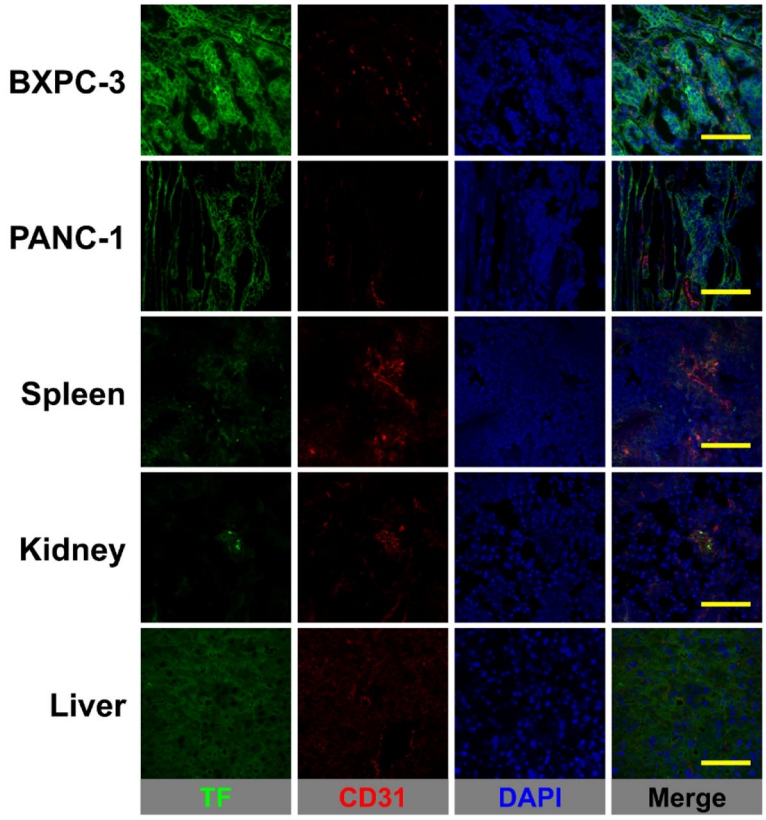


**Figure 5.**

TF/CD31 immunofluorescence co-staining of pancreatic tumors, spleen, kidney, and liver tissues. TF staining (green channel) was pronounced in BXPC-3 tumors whereas green fluorescence signal was at background levels in PANC-1 tumors, spleen, kidney, and liver. No significant overlap between CD31 (vasculature) and TF staining was observed. Scale bar = 50 μm.

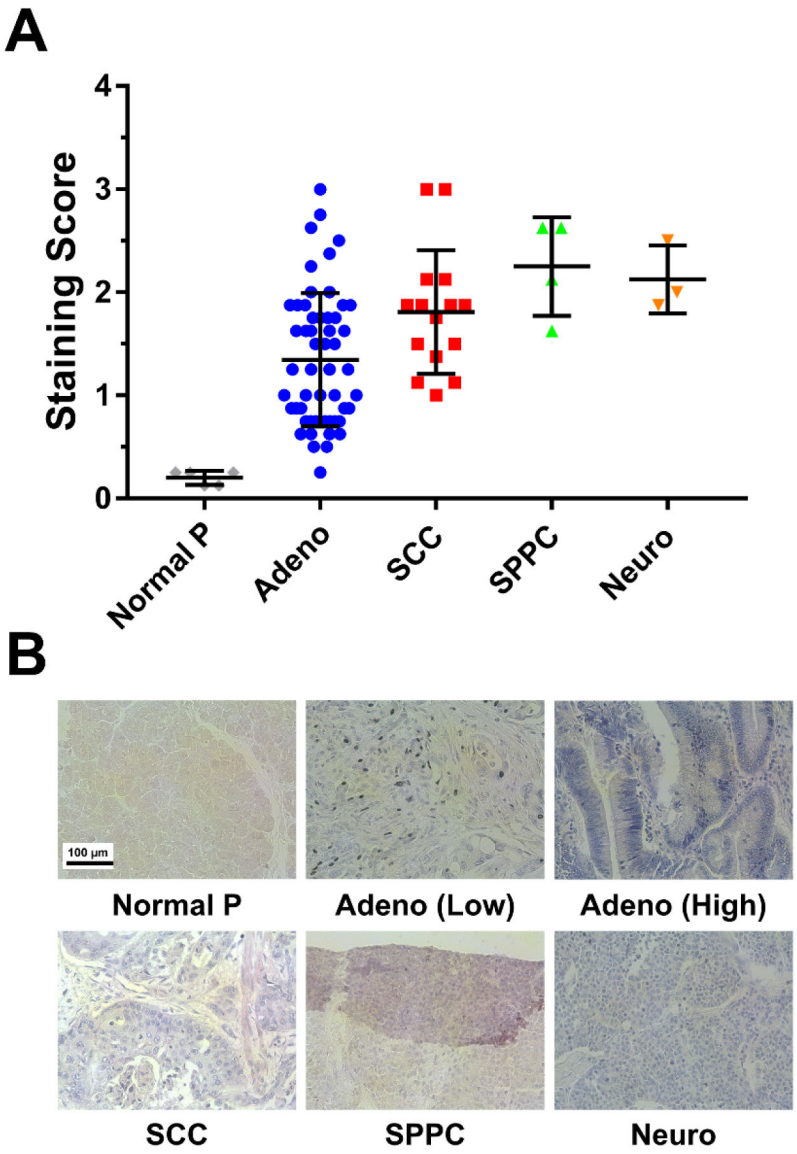


**Figure 6.**

Immunohistochemical analysis of TF expression in a human pancreatic cancer tissue microarray. **(A)** TF staining intensity scoring (range: 0 – 3) in different pancreatic cancer histological classification, and in healthy tissue. Markedly higher staining intensity scores were detected in tumor tissue compared to normal pancreas. **(B)** Representative stained slides for each of the tumor subtypes analyzed. TF expression is represented by the purple color. Normal pancreas: Normal P; pancreatic adenocarcinoma: Adeno; squamous cell carcinoma: SCC; solid pseudopapillary carcinomas: SPCC; neuroendocrine carcinomas: Neuro. Scale bar = 100 µm.